Available online at website: https://journal.bcrec.id/index.php/bcrec

Bulletin of Chemical Reaction Engineering & Catalysis, 22 (1) 2027, 119-133

Original Research Article

Hydrogenation of Palm Oil FAME into Fatty Alcohol using Pt/Sn-γ-Al_2O_3-B

Dede Sukandar[1,*], Wawan Rustyawan[2], Arini Fatikhatul Faqihah[1], Adawiah Adawiah[3,4], Tarso Rudiana[5], Suhendra Suhendra[6]

[1]*Department of Chemistry, Faculty of Science and Technology, UIN Syarif Hidayatullah Jakarta, Jl. Ir. H. Juanda No. 95, Ciputat, Tangerang Selatan 15412, Indonesia.*
[2]*Catalyst dan Materials, Research and Technology Innovation (RTI), Direktorat SPPU, PT Pertamina (Persero), Jalan Raya Bekasi Km 20, Pulogadung, Jakarta, Indonesia.*
[3]*Department of Chemistry, Faculty of Mathematics and Natural Sciences, University of Indonesia, Jl. Lingkar Kampus Raya, Pondok Cina, Beji, Depok, Jawa Barat, Indonesia.*
[4]*The Research Center for Polymer Technology, BRIN, 460th Building, B.J. Habibie Science and Technology Area Setu Sub-district, Tangerang Selatan, Banten, Indonesia.*
[5]*Department of Chemistry, Faculty of Science, Pharmacy and Health, Universitas Mathla'ul Anwar, Banten, Indonesia.*
[6]*Research and Publishing Center, LP2M, UIN Syarif Hidayatullah Jakarta, Jl. Ir. H. Juanda No. 95, Ciputat, Tangerang Selatan 15412, Indonesia.*

Received: 3rd October 2026; Revised: 12th November 2026; Accepted: 13th November 2026
Available online: 15th November 2026; Published regularly: April 2027

Abstract

Palm oil is an abundant resource in Indonesia that drives the development of the oleochemical industry, particularly the conversion of its derivative Fatty Acid Methyl Ester (FAME) into fatty alcohols used as raw materials for surfactants, lubricants, and cosmetics. FAME was chosen as a feedstock because it is more reactive for hydrogenation than direct triglycerides. This study examined the effect of tin (Sn) concentration (0.2, 0.4, 0.6%), which modifies platinum (Pt) structure through the ensemble effect, and boron (B) addition (0.3%) as a surface-acidity modulator, on the characteristics and activity of Pt/Sn-γ-Al_2O_3-B for FAME hydrogenation into fatty alcohol. Pt/Sn-γ-Al_2O_3-B catalysts were synthesized via sol-gel and dry impregnation, then characterized using XRD, XRF, Surface Area Analyzer (SAA), H_2-TPR, and NH_3-TPD. Activity tests were conducted in a fixed-bed reactor at 30 bar, 220-280 °C, LHSV of 1 h^{-1}, and H_2/HC ratio of 400 Nm^3/m^3. Products were analyzed with FTIR and GC-MS. Increasing Sn reduced crystallinity, crystal size, surface area, pore volume, and diameter, but raised the reduction temperature. The Pt/Sn(0.4)-γ-Al_2O_3-B at 260 °C achieved the highest FAME conversion (41.62%), though fatty alcohol selectivity and yield remained low (0.24% and 0.1%), as confirmed by the FTIR ester carbonyl absorption (1741-1743 cm^{-1}), indicating incomplete FAME conversion. The liquid product had an acid value of 11.97 mg/g, water content of 0.118 ppm, and density of 0.905 g/mL. Sn and B modifications improved catalyst properties, but carbonyl hydrogenation activity still requires further optimization.

Copyright © 2027 by Authors, Published by BCREC Publishing Group. This is an open access article under the CC BY-SA License (https://creativecommons.org/licenses/by-sa/4.0).

Keywords: FAME; fatty alcohol; hydrogenation; oleochemical; Pt/Sn-γ-Al_2O_3-B

How to Cite: Sukandar, D., Faqihah, A. F., Rustyawan, W., Adawiah, A., Rudiana, T., Suhendra, S. (2027). Hydrogenation of Palm Oil FAME into Fatty Alcohol using Pt/Sn-γ-Al_2O_3-B. *Bulletin of Chemical Reaction Engineering & Catalysis*, 22 (1), 119-133. (DOI: 10.9767/bcrec.20877)

Permalink/DOI: https://doi.org/10.9767/bcrec.20877

1. Introduction

Indonesia is the world's largest producer of crude palm oil (CPO), with production in 2025 reaching 51.66 million tons, up 7.26% from 48.164 million tons in 2024 [1]. Domestic oleochemical consumption also rose by 3.82%, from 23.859 million tons to 24.772 million tons [1], underscoring the need to enhance value addition through downstream sector development. One of the key products of the oleochemical industry is fatty alcohol, particularly the C12–C14 and C16–

* Corresponding Author.
Email: sukandarkimia@uinjkt.ac.id (D. Sukandar)

C18 carbon chains, which serve as essential components in surfactant, detergent, cosmetic, personal care, and lubricant formulations [2,3].

Commercially, fatty alcohol production from palm oil involves two main stages: transesterification of triglycerides into methyl esters [4], followed by catalytic hydrogenation into fatty alcohols [5]. Conventional hydrogenation employs copper–chromite (Cu–Cr) or Adkins catalysts, which are active and selective but pose environmental concerns due to hexavalent chromium (Cr^{6+}), classified as hazardous waste [6]. Moreover, these catalysts require extreme operating conditions (250–300 °C, 20–30 MPa H_2), leading to high energy consumption and safety risks [7].

Noble metal-based catalysts, particularly platinum (Pt) in bimetallic combinations, have demonstrated potential to operate at significantly lower temperatures and pressures than Cu–Cr while maintaining high conversion and selectivity. Zhang *et al.* reported that $PtSn/Al_2O_3$ converted acetic acid to ethanol with 90% conversion and 58.5% ethanol selectivity at 275 °C and 20 bar [8]. Pritchard *et al.* showed that Pt–Re/TiO_2 achieved 11% conversion of methyl hexanoate with 98% selectivity to 1-hexanol at 180 °C and 50 bar [9]. Brijaldo *et al.* demonstrated that $Pt/Nb_2O_5(1)/Al_2O_3$ converted furfural with 47% conversion and 99% selectivity to furfuryl alcohol [10], while Wang *et al.* reported a furfuryl alcohol yield of 87.6% using $Pt(1)–SnO_2(0.3)/Al_2O_3$ [11].

Modifiers such as tin (Sn) and boron (B) are frequently incorporated into noble metal catalysts to tailor metal functionality and catalyst acidity. Sánchez *et al.* reported that the addition of Sn and B to $Ru/\gamma\text{-}Al_2O_3$ enhanced the selectivity of FAME hydrogenation toward fatty alcohols [12]. The beneficial effect of Sn was attributed to a reduction in total acidity as well as suppression of dehydrogenation and hydrogenolysis activities, consistent with observations reported by Mazzieri *et al.* for $Ru\text{-}Sn/Al_2O_3$ catalysts [13]. In addition, Jiao *et al.* demonstrated that Sn promotes the formation of smaller Pt particles on Al_2O_3, thereby improving resistance to catalyst deactivation [14]. Boron, on the other hand, has been reported to decrease the concentration of Lewis acid sites on $\gamma\text{-}Al_2O_3$ and enhance resistance to coke formation [15]. Aly *et al.* further showed that boron forms amorphous oxide species dispersed over both the support and Pt particles, modifying the acidic properties of the support while simultaneously influencing the selectivity of metal sites [16].

Support acidity must be carefully controlled because it also influences cracking reactions. Taghizadeh Yusefabad *et al.* reported that the incorporation of borate into a $NiMo/ASA\text{-}Al_2O_3$ hydrocracking catalyst increased *n*-hexadecane conversion from 91.43% to 99.21%, which was attributed to enhanced acidic functionality [17]. On this basis, $Pt/Sn\text{-}\gamma\text{-}Al_2O_3\text{-}B$ catalysts containing a low Pt loading (0.1 wt%), 0.3 wt% B, with Sn loadings varied at 0.2, 0.4, and 0.6 wt%, were synthesised to optimise the balance between metallic and acidic functions for the hydrogenation of palm oil-derived FAME into fatty alcohols. The reaction was conducted in a continuous fixed-bed reactor at 30 bar. This study aimed to evaluate the effect of Sn loading on the physicochemical properties of the catalysts, including crystallinity, crystallite size, surface area, pore volume, pore diameter, total acidity, and reduction behaviour. The influence of reaction temperature (220, 240, 260, and 280 °C) on FAME conversion and fatty alcohol selectivity was also investigated.

2. Materials and Method

2.1. Materials

The materials used included boehmite (AlO(OH)) from PT Pertamina, distilled water, HNO_3 65% (pro-analysis Merck, 65%), NH_4OH 25% (pro-analysis Merck, 99.9%), $SnCl_2.2H_2O$ (E-Merck Germany, 99.9%), H_3BO_3 (E-Merck Germany, 99.5%), KOH 0.1 N in isopropyl alcohol (pro-analysis Merck), α-naphtholbenzein, 2-propanol (pro-analysis Merck, ≥99.8%), toluene (pro-analysis Merck, ≥99.9%), tetraammineplatinum(II) nitrate ($[Pt(NH_3)_4](NO_3)_2$ Sigma-Aldrich, 99.995%), palm oil FAME supplied by PT Pertamina, as well as oxygen, hydrogen, nitrogen gases from SAMATOR.

2.2. Synthesis of $Pt/Sn\text{-}\gamma\text{-}Al_2O_3$–B Catalyst

The catalyst was synthesized through a combination of the sol-gel and dry impregnation methods. Boehmite was mixed with H_3BO_3 (0.3 wt% B) and $SnCl_2 \cdot 2H_2O$ solution (Sn variations of 0.2, 0.4, and 0.6 wt%), along with 5% HNO_3 as a peptizing agent; 25% NH_4OH was then added to initiate condensation and gel formation. The mixture was shaped using an extruder and calcined stepwise at 150 °C for 1 hour, 250 °C for 1 hour, and 550 °C for 5 hours, yielding the $Sn\text{-}\gamma\text{-}Al_2O_3\text{-}B$ support. The support was subsequently impregnated with $[Pt(NH_3)_4](NO_3)_2$ solution (target Pt content of 0.1 wt%) via the dry impregnation method, then calcined stepwise at 150 °C under air flow for 1.5 hours to prevent agglomeration, followed by calcination without air flow at 250 °C for 1 hour and 450 °C for 3 hours, yielding the $Pt/Sn\text{-}\gamma\text{-}Al_2O_3\text{-}B$ catalyst. A $Pt/\gamma\text{-}Al_2O_3\text{-}Cl$ reference catalyst was used for comparison [18].

Copyright © 2027, ISSN 1978-2993

2.3. Catalyst Characterizations

Crystallinity, crystal size, and crystal phases were analyzed using X-ray Diffraction (XRD, Malvern PANalytical Empyrean) with Cu radiation (40 kV, 35 mA) over a 2θ range of 5°–90°, following ASTM D4926-20. Crystal size was calculated using the Debye–Scherrer equation. Elemental composition was determined by X-ray Fluorescence (XRF, Malvern PANalytical Axios) at 40 kV and 45 mA (ASTM D7343-20). Surface area, pore volume, and pore diameter were measured using a Surface Area Analyzer (Quantachrome AUTOSORB-6B) via the BET method and nitrogen adsorption–desorption, in accordance with ASTM D3663-20, ASTM D4222-20, and ASTM D4641-17. Catalyst reduction temperature was analyzed by Temperature-Programmed Reduction (H_2-TPR, Quantachrome ChemBET Pulsar) using 4% H_2 in Ar as the carrier gas, with a heating rate of 10 °C/min up to 600 °C (ASTM D7442-22). Total acidity was determined by Temperature-Programmed Desorption (NH_3-TPD, Quantachrome ChemBET Pulsar), with stepwise He desorption up to 800 °C after NH_3 adsorption at room temperature (ASTM D4824-24).

2.4. Catalyst Performance Test

Catalytic performance was evaluated in a pilot-scale fixed-bed reactor (XYTEL NX-3) loaded with 50 cc of catalyst. Prior to reaction, the system was purged with N_2, followed by catalyst activation under H_2 flow. Hydrogenation of palm oil-derived FAME was carried out at an LHSV of 1 h^{-1}, a pressure of 30 bar, and an H_2/HC ratio of 400 Nm^3/m^3. The reactor was operated continuously at 220, 240, 260, and 280 °C in sequence. Following each temperature adjustment, the system was maintained for 24 h to achieve steady-state operation, and liquid products were collected at 8 h intervals. Samples obtained during the final 8 h period at each temperature were used for product distribution analysis. For comparison, the Pt/γ-Al_2O_3-Cl catalyst was evaluated at 220, 240, and 260 °C with an H_2/HC ratio of 200 Nm^3/m^3, as well as at 260 °C with an H_2/HC ratio of 400 Nm^3/m^3 [18].

2.5. Product Analysis

The liquid products obtained from the hydrogenation reaction were analyzed using Gas Chromatography–Mass Spectrometry (GC–MS, Agilent 8890). The GC peak area percentages were initially assumed to be proportional to the mass fractions of the respective compounds, providing a semi-quantitative estimation of the product composition. To determine the molar composition, the relative molar amount of each compound was calculated by dividing its GC peak area by its corresponding molecular weight (MW), followed by normalization against the total relative molar amounts of all identified compounds, as presented in Equation (1). The resulting molar percentages were subsequently used to calculate FAME conversion, fatty alcohol selectivity, and product yield according to Equations (2–4):

$$Mol_i\ (\%) = \frac{\frac{Ai}{Mwi}}{\sum_{j=1}^{n}\left(\frac{Aj}{MWj}\right)} \times 100\% \quad (1)$$

$$\text{Conversion}\ (\%) = \frac{n\text{FAME}_{\text{initial}} - n\text{FAME}_{\text{final}}}{n\text{FAME}_{\text{initial}}} \times 100\% \quad (2)$$

$$Selectivity\ (\%) = \frac{nfatty\ alcohol}{n\text{FAME}_{\text{initial}} - n\text{FAME}_{\text{final}}} \times 100\% \quad (3)$$

$$Yield\ (\%) = \frac{(\%\text{selectivity} \times \%\text{conversion})}{100} \quad (4)$$

where, A_i is GC peak area of the i^{th} component, and MW_i is molar mass of the i^{th} component.

Functional groups of the products were identified using Fourier Transform Infrared Spectroscopy (FTIR, Agilent Cary 630) within the range of 4000–400 cm^{-1} (ASTM E1252-98). Water content was determined using a UHV-660 Automatic Coulometric Karl Fischer Titrator (ASTM D6304-20). The total acid number was measured via titration with 0.1 N KOH using α-naphtholbenzein as an indicator (ASTM D974-22). Product density was determined using a pycnometer 25 mL at 25 °C (ASTM D1475-13).

3. Results and Discussion

3.1. Pt/Sn-γ-Al_2O_3-B Catalyst

Catalyst synthesis via the sol-gel method began with the protonation of surface hydroxyl groups on boehmite with HNO_3, forming a colloidal sol, followed by interparticle condensation induced by NH_4OH, forming a gel network in which Sn and B were dispersed. Stepwise calcination transformed the boehmite into the transitional γ-Al_2O_3 phase, with Sn and B trapped within the crystal framework. Impregnation of the $[Pt(NH_3)_4]^{2+}$ complex occurred through strong electrostatic adsorption onto the negatively charged support surface. In summary, the catalyst formation stages can be represented by the following reaction equations. Peptization and gel condensation (formation of the Sn-γ-Al_2O_3-B support):

$$Al–OH + H^+ \rightarrow Al–OH_2^+$$
$$Al–OH + Sn(OH)_2 \rightarrow Al–O–Sn–OH + H_2O$$
$$Al–OH + B(OH)_4^- \rightarrow Al–O–B(OH)_3^- + H_2O$$
$$Al–O–Sn–OH + Al–O–B(OH)_3^- \xrightarrow{\Delta\ (550\ ℃)} \text{Sn-}\gamma\text{-}Al_2O_3\text{-B} + H_2O\uparrow$$

Copyright © 2027, ISSN 1978-2993

Impregnation and formation of the Pt/Sn-γ-Al_2O_3-B catalyst:

$(Sn\text{-}\gamma\text{-}Al_2O_3\text{-}B)\text{–}OH \rightarrow (Sn\text{-}\gamma\text{-}Al_2O_3\text{-}B)\text{–}O^- + H^+$

$2(Sn\text{-}\gamma\text{-}Al_2O_3\text{-}B)\text{–}O^- + [Pt(NH_3)_4]^{2+} \rightarrow [(Sn\text{-}\gamma\text{-}Al_2O_3\text{-}B)\text{–}O]_2Pt(NH_3)_4$

$[(Sn\text{-}\gamma\text{-}Al_2O_3\text{-}B)\text{–}O]_2Pt(NH_3)_4 + xO_2 \xrightarrow{\Delta} PtO_x/Sn\text{-}\gamma\text{-}Al_2O_3\text{-}B + N_2\uparrow + H_2O\uparrow$

3.2. Crystallinity, Crystal Size, and Crystal Phase

The crystal phase, crystallite size, and crystallite size were analyzed using XRD. The results are presented in Figure 1 and Table 1. XRD analysis revealed the characteristic diffraction peaks of γ-Al_2O_3 at 2θ values of 37.44°, 45.81°, and 66.73°, which are consistent with ICDD No. 01-079-1558. The incorporation of Sn, B, and Pt did not produce additional crystalline phases or detectable peak shifts, indicating that these species were not incorporated into the alumina lattice and were instead highly dispersed on the support surface [19–23]. The absence of diffraction peaks associated with Sn, B, and Pt may also be attributed to crystallite sizes below the XRD detection limit because of the low metal loadings employed [21,23,24]. For the Pt/γ-Al_2O_3-Cl catalyst, diffraction peaks assigned to gibbsite were observed at 2θ values of 18.28° and 20.28°, possibly originating from the partial hydrolysis of Al^{3+} species during impregnation with the acidic H_2PtCl_6 precursor. In addition, no Pt-related diffraction peak was observed in the 2θ range of 81-82°, suggesting that Pt remained highly dispersed and did not undergo significant agglomeration in any of the catalysts studied [20,24]. Crystallite size and crystallinity data are presented in Table 1.

During calcination, γ-Al_2O_3 crystallite growth occurs through the condensation of Al-OH groups into Al-O-Al linkages and sintering induced by surface dehydroxylation [25,26]. The addition of Sn and B inhibited these processes, consistent with previous reports showing that oxide dopants and boron enhance the sintering resistance of alumina and suppress crystallisation [27–29]. As a result, the crystallite size decreased from 3.82 nm for γ-Al_2O_3 to 3.48, 3.02, and 3.26 nm for Sn(0.2)- γ-Al_2O_3-B, Sn(0.4)-γ-Al_2O_3-B, and Sn(0.6)-γ-Al_2O_3-B, respectively, accompanied by a reduction in crystallinity from 45.53% to 42.37-40.78%. Following Pt impregnation, the crystallite size remained

Table 1. Crystallite size and crystallinity data.

Sample	Crystal Size (nm)	Crystallinity (%)
γ-Al_2O_3	3.82	45.53
Sn(0.2)-γ-Al_2O_3-B	3.48	42.37
Sn(0.4)-γ-Al_2O_3-B	3.02	40.90
Sn(0.6)-γ-Al_2O_3-B	3.26	40.78
Pt/Sn(0.2)-γ-Al_2O_3-B	3.30	42.78
Pt/Sn(0.4)-γ-Al_2O_3-B	3.24	44.12
Pt/Sn(0.6)-γ-Al_2O_3-B	3.35	44.86
Pt/γ-Al_2O_3-Cl	3.81	41.16

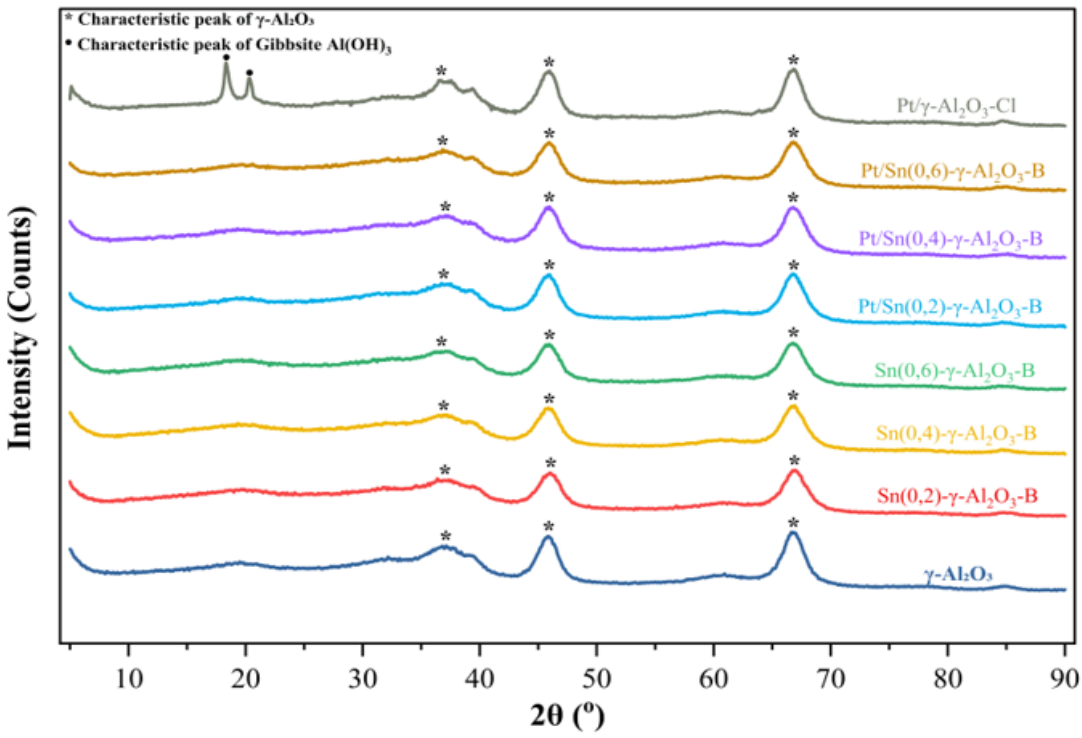


Figure 1. Diffraction pattern of catalysts

Copyright © 2027, ISSN 1978-2993

within the range of 3.30-3.35 nm, with crystallinity values of 42.78-44.86%, whereas Pt/γ-Al_2O_3-Cl exhibited a crystallite size of 3.81 nm and a crystallinity of 41.16%. The relatively small crystallite sizes indicate good structural stability, which may contribute to maintaining active metal dispersion and suppressing sintering under high-temperature reaction conditions [30–32].

3.3. Elemental Composition of the Support and Catalyst

The elemental composition of the support and catalyst was analyzed using XRF. The results are presented in Table 2. XRF analysis showed that the synthesized catalysts achieved the target metal loadings of Pt (0.1%) and Sn (0.2%, 0.4%, and 0.6%). Boron doping formed B–O–Al bonds on the alumina surface, thereby stabilizing the Pt–B interaction, preserving Pt dispersion, and suppressing sintering. The addition of boron, together with Sn lowered the point of zero charge (PZC) of the support to slightly acidic [33], so that impregnation with the basic $Pt(NH_3)_4^{2+}$ precursor rendered the support surface negatively charged and accelerated deposition of the cationic Pt complex. Boron was not detected by XRF because its Kα X-ray energy is very low (183 eV), and standard XRF is not designed to detect elements below Na (Z = 11) [34]; quantification of boron requires the more sensitive ICP-OES instrument for light elements [35].

3.4. Pore Diameter, Pore Volume, and Surface Area

Pore diameter, pore volume, and surface area of the catalysts were analyzed using the BET method with a Surface Area Analyzer (SAA) instrument, using nitrogen gas as the adsorbate. The results are presented in Table 3. The addition of Sn and boron increased the surface area from 230.63 m^2/g (pure γ-Al_2O_3) to 292.45 m^2/g for Sn(0.2)-γ-Al_2O_3-B, while Sn contents of 0.4 and 0.6% resulted in a relatively stable surface area (286.43–287.32 m^2/g), indicating that boron acted as a textural promoter that inhibited sintering. Pt impregnation did not cause any significant change (287.16–294.43 m^2/g). Pore diameter decreased with increasing Sn content, while surface area and pore volume initially rose before declining again; the Sn–B complex acted as a partial substituent for Al^{3+} ions, inducing lattice defects and refining the mesoporous structure [19]. The reference catalyst Pt/γ-Al_2O_3-Cl, without Sn and B, exhibited the lowest surface area (224.35 m^2/g), confirming the effectiveness of the Sn-B combination in preserving surface area and supporting active-site dispersion. All samples had pore diameters within the mesoporous range (2–50 nm), suitable for minimizing internal diffusion resistance in the FAME hydrogenation reaction [36,37].

Table 2. XRF analysis results. (Note: -* not detected (boron below the XRF detection limit)

Sample	Pt (%)	Sn (%)	B (%)	Cl (%)
Sn(0.2)-γ-Al_2O_3-B	-	0.19	-*	-
Sn(0.4)-γ-Al_2O_3-B	-	0.42	-*	-
Sn(0.6)-γ-Al_2O_3-B	-	0.58	-*	-
Pt/Sn(0.2)-γ-Al_2O_3-B	0.18	0.27	-*	-
Pt/Sn(0.4)-γ-Al_2O_3-B	0.21	0.52	-*	-
Pt/Sn(0.6)-γ-Al_2O_3-B	0.17	0.66	-*	-
Pt/γ-Al_2O_3-Cl	0.85	-	-*	0.71

Table 3. BET analysis results.

Sample	Average Pore Diameter (nm)	Pore Volume (cm^3/g)	Surface Area (m^2/g)
γ-Al_2O_3	5.703	0.3288	230.63
Sn(0.2)-γ-Al_2O_3-B	5.045	0.3688	292.45
Sn(0.4)-γ-Al_2O_3-B	5.041	0.3608	286.43
Sn(0.6)-γ-Al_2O_3-B	5.016	0.3603	287.32
Pt/Sn(0.2)-γ-Al_2O_3-B	5.083	0.3657	287.82
Pt/Sn(0.4)-γ-Al_2O_3-B	4.99	0.3676	294.43
Pt/Sn(0.6)-γ-Al_2O_3-B	5.001	0.359	287.16
Pt/γ-Al_2O_3-Cl	11.66	0.654	224.35

Copyright © 2027, ISSN 1978-2993

3.5. Catalyst Reduction Temperature

The catalyst reduction temperature was analyzed using a Chemisorption Analyzer to determine shifts in the reduction peaks, which indicate metal–support interactions and the degree of difficulty in reducing the oxides. A graph of the reduction temperature analysis results is shown in Figure 2. Pt reduction occurred in all catalysts but was strongly influenced by the presence of Sn. In the Pt/γ-Al_2O_3-Cl, the dominant reduction peak appeared at a high temperature (358.96 °C) due to stable Pt-oxychloride species. At low Sn content (0.27%), the reduction temperature shifted to a lower value (323.16 °C) due to Pt–Sn interactions that facilitated hydrogen spillover. Medium (0.52%) and high (0.66%) Sn contents shifted the main reduction to higher temperatures (385.04 and 596.52 °C), as a thicker SnO_x layer covered the Pt and hindered hydrogen diffusion [38,39]. Overall, Sn played a dual role: enhancing hydrogen spillover at low content but inhibiting it at high content.

3.6. Total Catalyst Acidity

Total catalyst acidity was analyzed using a Chemisorption Analyzer. The results showed strong, medium, and weak acid sites, as presented in Table 4. γ-Al_2O_3 exhibits moderate-to-strong acidity that originates primarily from Lewis acid sites associated with three-coordinate Al defect species [14,40]. As shown in Table 4, these two types of acid sites were detected at desorption temperatures of 258.6 and 811.1 °C, giving a total acidity of 0.11 mmol.g^{-1}. The reference Pt/γ-Al_2O_3-Cl catalyst (0.71 wt% Cl) exhibited the highest total acidity (1.541

Table 4. H_2-TPR graph of catalysts

Sample	Desorption Temperature (°C)	Acid Site (mmol/g)			Total Acid (mmol/g)
		Weak	Medium	Strong	
γ-Al_2O_3	258.6	-	0.055	-	0.11
	811.1	-	-	0.055	
Pt/Sn(0.2)-γ-Al_2O_3-B	284.6	-	0.115	-	0.132
	354.5	-	0.017	-	
Pt/Sn(0.4)-γ-Al_2O_3-B	241.8	-	0.596	-	0.929
	809.8	-	-	0.333	
Pt/Sn(0.6)-γ-Al_2O_3-B	254.7	-	0.022	-	0.276
	703.7	-	-	0.078	
	803.4	-	-	0.176	
Pt/γ-Al_2O_3-Cl	296.1	-	0.153	-	1.541
	707.3	-	-	0.883	
	821.8	-	-	0.505	

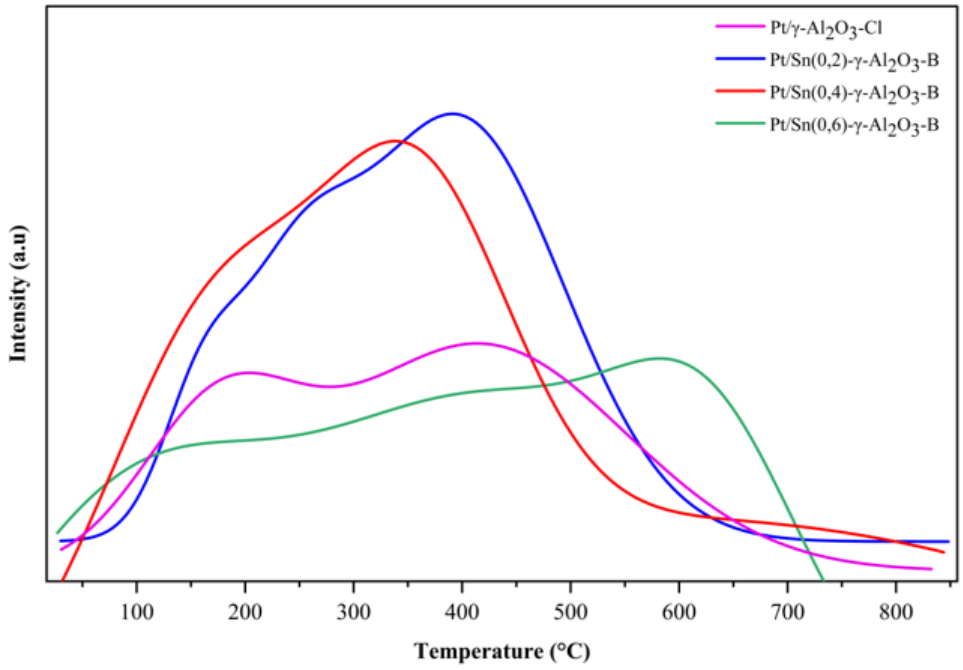


Figure 2. H_2-TPR graph of catalysts

Copyright © 2027, ISSN 1978-2993

mmol.g^{-1}) and was dominated by strong acid sites, consistent with the increased surface electronegativity resulting from the substitution of surface OH groups by Cl species [41,42]. For the Pt/Sn-γ-Al_2O_3-B catalysts (0.3 wt% B), the effect of Sn loading on acidity was non-monotonic. At 0.27 wt% Sn, strong acid sites were not detected, whereas the concentration of moderate acid sites increased to 0.132 mmol.g^{-1}. This behaviour suggests that Sn and B contribute to the suppression of strong acidity on alumina [14,16,43], while SnO_x species may promote the formation of moderate Lewis acid sites [14].

Increasing the Sn loading to 0.52 wt% raised the total acidity to 0.929 mmol.g^{-1}, comprising 0.596 mmol.g^{-1} moderate acid sites and 0.333 mmol.g^{-1} strong acid sites. This result is consistent with reports on Sn-Al_2O_3 systems, where SnO_x species containing Sn^{4+} act as additional Lewis's acid centres and can generate stronger acid sites than those present on bare alumina [14,44]. These findings indicate that the influence of Sn on acidity depends strongly on both catalyst composition and metal loading. At 0.66 wt% Sn, the contribution of moderate acid sites decreased to 0.022 mmol.g^{-1}, whereas strong acid sites remained dominant (0.254 mmol.g^{-1}, with desorption peaks at 703.7 and 803.4 °C), suggesting that surface SnO_x species serve as a source of strong acidity [44]. Despite the predominance of strong acid sites, the total acidity decreased to 0.276 mmol.g^{-1}, indicating partial coverage of alumina acid sites by SnO_x species at higher Sn loadings [45,46]. It should be noted that NH_3-TPD cannot differentiate between Lewis and Brønsted acid sites. Therefore, acid-site assignments were made based on previous literature reports [14].

3.7. Catalyst Activity Test: Conversion and Selectivity

The Pt/Sn(0.4)-γ-Al_2O_3-B catalyst was selected as the best variation for its highest Pt content (0.21%) among the three synthesis variations tested and was subsequently used in the FAME feedstock conversion process. The FAME feedstock composition, analyzed by GC-MS, is presented in Table 5. The reference

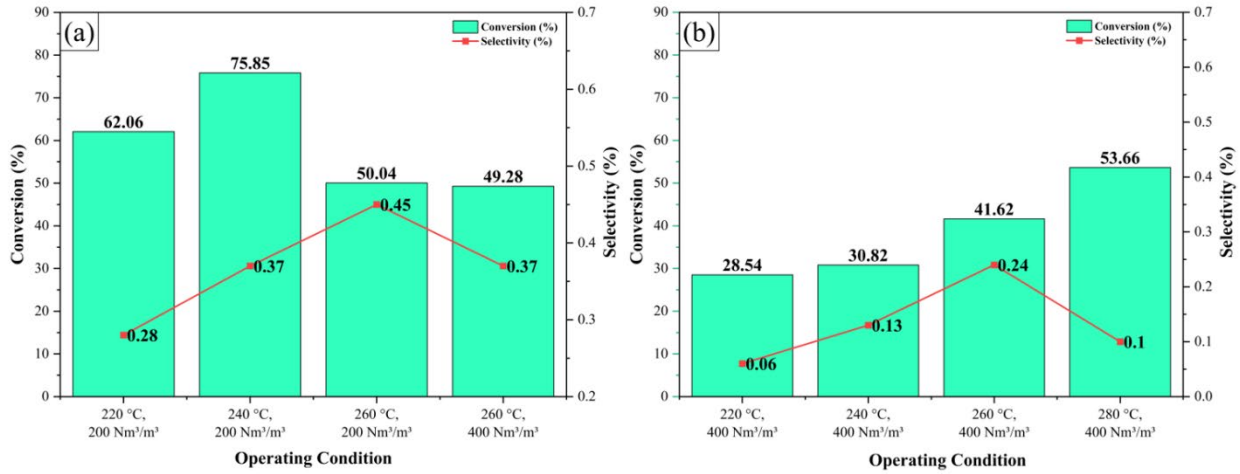


Figure 3. Conversion and selectivity: (a) Pt/γ-Al_2O_3-Cl (b) Pt/Sn(0.4)-γ-Al_2O_3-B.

Table 5. FAME feedstock composition.

Feedstock Composition (Reference)			Feedstock Composition (Synthesis)		
Area (%)	Compound	Formula	Area (%)	Compound	Formula
0.22	Dodecanoic acid, methyl ester	$C_{13}H_{26}O_2$	0.23	Dodecanoic acid, methyl ester	$C_{13}H_{26}O_2$
1.14	Methyl tetradecanoate	$C_{15}H_{30}O_2$	1.34	Methyl tetradecanoate	$C_{15}H_{30}O_2$
-			11.64	Tetradecanoic acid, 12-methyl-, methyl ester	$C_{16}H_{32}O_2$
0.12	Heptadecanoic acid, methyl ester	$C_{18}H_{36}O_2$	0.91	Heptadecanoic acid, methyl ester	$C_{18}H_{36}O_2$
-			5.21	9,12-Octadecadienoic acid, methyl ester	$C_{19}H_{34}O_2$
4.24	Methyl stearate	$C_{19}H_{38}O_2$	6.23	Methyl stearate	$C_{19}H_{38}O_2$
7.52	11-Octadecenoic acid, methyl ester	$C_{19}H_{36}O_2$	15.96	9-Octadecenoic acid (Z)-, methyl ester	$C_{19}H_{36}O_2$
12.49	9-Octadecenoic acid (Z)-, methyl ester	$C_{19}H_{36}O_2$	30.79	9-Octadecenoic acid, methyl ester, (E)-	$C_{19}H_{36}O_2$
22.81	Eicosanoic acid, methyl ester	$C_{21}H_{42}O_2$	24.58	Eicosanoic acid, methyl ester	$C_{21}H_{42}O_2$
-			0.15	8,11,14-Docosatrienoic acid, methyl ester	$C_{23}H_{40}O_2$

Copyright © 2027, ISSN 1978-2993

catalyst's FAME feedstock (total area 48.53%) was dominated by eicosanoic acid methyl ester, 9- and 11-octadecenoic acid methyl esters, and methyl stearate, while the synthesized catalyst's feedstock (total area 97.05%) was dominated by (E)-9-octadecenoic acid methyl ester, eicosanoic acid methyl ester, and (Z)-9-octadecenoic acid methyl ester.

FAME conversion over the Pt/γ-Al_2O_3-Cl catalyst (Figure 3) increased from 62.06% (220 °C) to a peak of 75.85% (240 °C), then declined to 50.04% (260 °C) and 49.28% when the H_2 ratio was increased (400 Nm^3/m^3), indicating catalyst deactivation caused by strong acid sites that promoted hydrodeoxygenation and coking [47,48]. In contrast, the Pt/Sn(0.4)-γ-Al_2O_3-B catalyst, with lower strong-acid-site content, showed a continuously increasing conversion trend up to 53.66% at 280 °C, reaching a maximum conversion of 41.62% at 260 °C, supported by the low water content of the feedstock, which kept the acid and metal sites active.

Fatty alcohol selectivity was low for both catalysts, indicating the dominance of side reactions. For Pt/γ-Al_2O_3-Cl, selectivity increased from 0.28% (220 °C) to a peak of 0.45% (260 °C), then decreased to 0.37% when the H_2 ratio was increased, due to excess H_2 promoting further hydrodeoxygenation into hydrocarbons [47]. For Pt/Sn(0.4)-γ-Al_2O_3-B, selectivity increased from 0.06% (220 °C) to a peak of 0.24% (260 °C), then decreased to 0.10% (280 °C) due to condensation into wax esters and ethers. For comparison, Sánchez *et al.* [49] reported that a Ru(1%)-Sn(2%)-B/γ-Al_2O_3 catalyst achieved 45% oleyl alcohol selectivity under harsher conditions (290 °C, 50 atm), attributed to Ru^+-SnO_x active sites that more selectively activated carbonyl groups.

The metal-specific efficiency (fatty alcohol yield per percent of total active metal) for the Pt/γ-Al_2O_3-Cl catalyst reached 32.65% (240 °C, 200 Nm3/m3) with a yield of 0.28% (Table 6), supported by a high Pt content (0.85%) and strong acidity (1.388 mmol/g) resulting from the chlorine additive, which activated the C=O bond [50]. The Pt/Sn(0.4)-γ-Al_2O_3-B catalyst (total active metal content of 0.73%: Pt 0.21%, Sn 0.52%), with more moderate acidity, achieved only a maximum yield of 0.1% (260 °C) and an efficiency of 13.41% (Table 2), as the oxophilic Sn was less effective at activating hydrogen compared to Pt [51]. Fonseca Benítez *et al.* [52] reported that a Rh-Sn-B/γ-Al_2O_3 catalyst produced oleyl alcohol yields of up to 85.5%, indicating that considerable room for optimization remains open for the PtSnB system.

The by-product distribution of the Pt/γ-Al_2O_3-Cl was dominated by alkanes and aromatic hydrocarbons resulting from hydrodeoxygenation (Figure 4a), along with ester isomers produced by Pt-catalyzed isomerization of C=C double bonds [53,54]. By contrast, Pt/Sn(0.4)-γ-Al_2O_3-B predominantly produced wax esters, ethers, and aldehydes as by-products, with only minor amounts of alkanes, alkenes, and ester isomers (Figure 4b). The wax esters were generated via transesterification of fatty alcohols with FAME (or by esterification with fatty acids) on strong acid sites (0.333 $mmol.g^{-1}$), and their reconversion

Table 6. Fatty alcohol yield and metal-specific efficiency.

Sample	*Fatty alcohol* yield (%)	Metal-specific efficiency (%)
$T_{220\ °C,\ 200\ Nm^3/m^3}$	0.17	20.33
$T_{240\ °C,\ 200\ Nm^3/m^3}$	0.28	32.65
$T_{260\ °C,\ 200\ Nm^3/m^3}$	0.23	26.48
$T_{260\ °C,\ 400\ Nm^3/m^3}$	0.18	21.45
$T_{220\ °C,\ 400\ Nm^3/m^3}$	0.02	2.37
$T_{240\ °C,\ 400\ Nm^3/m^3}$	0.04	5.63
$T_{260\ °C,\ 400\ Nm^3/m^3}$	0.10	13.41
$T_{280\ °C,\ 400\ Nm^3/m^3}$	0.05	7.52

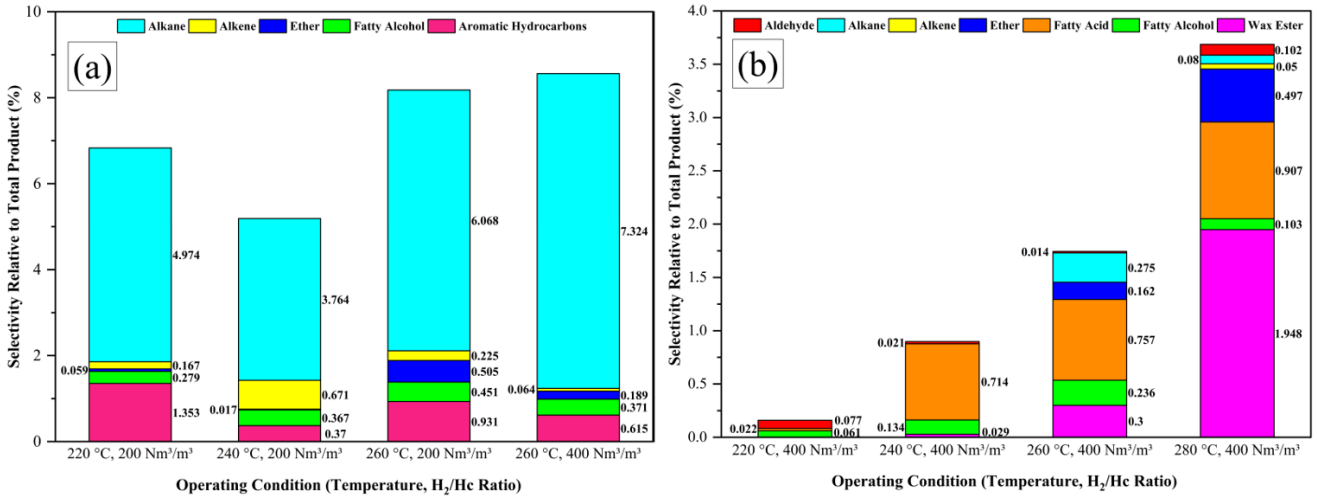


Figure 4. By-product distribution: (a) Pt/γ-Al_2O_3-Cl (b) Pt/Sn(0.4)-γ-Al_2O_3-B.

Copyright © 2027, ISSN 1978-2993

to fatty alcohols by hydrogenolysis remained incomplete at 30 bar H_2 [55]. Ethers were generated through intermolecular dehydration of fatty alcohols on medium-strength acid sites (0.596 mmol.g^{-1}), the highest value observed among the Sn-containing catalysts. Aldehydes were detected as intermediates during ester hydrogenation, and their persistence suggests incomplete conversion to fatty alcohols, likely due to fewer accessible Pt sites in the presence of Sn. The concurrent formation of wax esters and the persistence of aldehydes further point to a low hydrogen concentration at the catalyst surface. Hydrogen, being a small nonpolar molecule, has limited solubility in oxygenated organic media, and its solubility is influenced by pressure and temperature [56–59]. The low levels of alkanes and alkenes suggest that C–O hydrogenolysis and intramolecular dehydration are limited over this catalyst, which agrees with the reduced alkane formation reported at moderate temperatures for Ru-Sn-B/Al_2O_3 [12]. However, because the two catalysts differ in Pt loading (0.21 vs 0.85 wt%), Sn content, Cl content, and acidity, the observed differences in by-product distribution cannot be ascribed to a single variable.

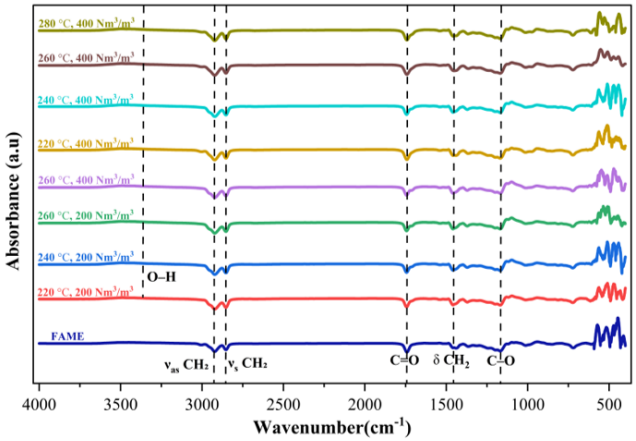


Figure 5. FTIR spectrum of the fatty alcohol product.

3.8. Product Functional Group Analysis (FTIR)

The functional groups of the fatty alcohol product were analyzed using FTIR, with the results presented in Figure 5. The FTIR spectrum of the hydrogenation product showed a broad, strong absorption band at 3350.41–3355.23 cm^{-1}, evidence of the formation of hydroxyl (O–H) groups characteristic of alcohols. Asymmetric (2922.21–2923.17 cm^{-1}) and symmetric (2852.77–2853.73 cm^{-1}) C–H absorptions indicated long alkyl chains. The absence of absorption at 3000–3100 cm^{-1} (=C–H) or 1650 cm^{-1} (C=C) indicated that the double bonds in the FAME had been hydrogenated into unsaturated chains. However, a sharp band at 1741.75–1743.68 cm^{-1} (ester C=O), reinforced by the absorption at 1168.88 cm^{-1} (asymmetric C–O of O–CH_3), indicated that a substantial amount of FAME had not yet been fully converted into fatty alcohol, since pure fatty alcohol typically absorbs at a lower wavenumber for primary alcohol C–O (1000–1075 cm^{-1}) [60–62].

3.9. Water content of Product

The water content of the fatty alcohol product was analyzed using a Karl Fischer instrument. The results are presented in Table 7. The fatty alcohol product from the synthesized catalyst had a much lower water content compared to that from the reference catalyst. The water content of the Pt/γ-Al_2O_3-Cl catalyst product increased with rising operating temperature, consistent with the presence of residual fatty acid in the feedstock and the dominance of strong acid sites, which promoted the hydrogenation of fatty acid, with water as a by-product. In contrast, the feedstock for the Pt/Sn(0.4)-γ-Al_2O_3-B catalyst contained almost no fatty acid (0.09% area), so the water content of the product did not differ significantly from that of the feedstock; the increase in water content at higher temperatures was instead attributed to the condensation of fatty alcohol to form ethers and dehydration reactions forming alkenes that released water [63].

Table 7. Water content analysis results.

Operating Conditions		Water Content (ppm)	
H_2/Hc (Nm^3/m^3)	Temperature (°C)	Pt/γ-Al_2O_3-Cl	Pt/Sn(0.4)-γ-Al_2O_3-B
Feed		893.833	0.135
200	220	624.850	-
	240	693.165	-
	260	814.349	-
400	220	-	0.173
	240	-	0.116
	260	1517.900	0.118
	280	-	0,154

Copyright © 2027, ISSN 1978-2993

3.10. Total Acid Number of the Product

The total acid number of the product was determined by titration with a 0.1 N KOH titrant and α-naphtholbenzoin indicator. The results of the total acid number analysis are presented in Figure 6. The total acid number of the product was positively correlated with the fatty acid-to-catalyst acidity ratio. The Pt/γ-Al_2O_3-Cl catalyst, with higher strong acid sites and a feedstock fatty acid content of 6.67% area, produced a higher total acid number in the product, whereas the Pt/Sn-γ-Al_2O_3-B catalyst, with feedstock fatty acid content that was almost negligible (0.09% area), showed an increase in fatty acid with rising temperature due to in situ water rehydrolysis of the FAME [64].

3.11. Density of Products

The density of the fatty alcohol product was analyzed using a pycnometer 25 mL at 25 °C. The results are presented in Table 8. Product density analysis showed that product density was generally lower than that of the FAME feedstock, consistent with loss of the methoxy group (–OCH_3) as methanol during ester-to-alcohol conversion [65]. For the Pt/Sn(0.4)-γ-Al_2O_3-B catalyst, density dropped sharply from 0.913 g/mL (feedstock) to 0.880 g/mL at 220 °C, reflecting dominant double-bond isomerization that disrupted molecular regularity, then gradually rose to 0.906 g/mL at 280 °C as heavier wax esters formed via condensation of FAME or fatty acids with fatty alcohol [66].

3.12. FAME Hydrogenation Mechanism

The FAME hydrogenation reaction began with the activation of hydrogen gas on the Pt surface, facilitating its dissociation into H atoms, while the carbonyl group (C=O) was activated by adsorption at catalyst sites (Figure 7). In the reference catalyst, the carbonyl group interacted with Lewis acid Al^{3+} sites whose acidity was enhanced by chlorine, whereas in the Pt/Sn(0.4)-γ-Al_2O_3-B catalyst, the carbonyl group was adsorbed by the oxophilic Sn, while boron modulated the surface acidity without acting as a direct adsorption site. The weakened C=O bond was then attacked by H atoms adsorbed on Pt, producing aldehyde (RCHO) and methanol (CH_3OH) intermediates, which were subsequently further hydrogenated into fatty alcohol (RCH_2OH) [49,67].

Table 8. The density of FAME hydrogenation product.

Operating Conditions		Density (g/mL)	
H_2/Hc (Nm^3/m^3)	Temperature (°C)	Pt/γ-Al_2O_3-Cl	Pt/Sn(0.4)-γ-Al_2O_3-B
Feed		0.897	0.913
200	220	0.897	-
	240	0.888	-
	260	0.881	-
400	220	-	0.880
	240	-	0.905
	260	0.877	0.906
	280	-	0.896

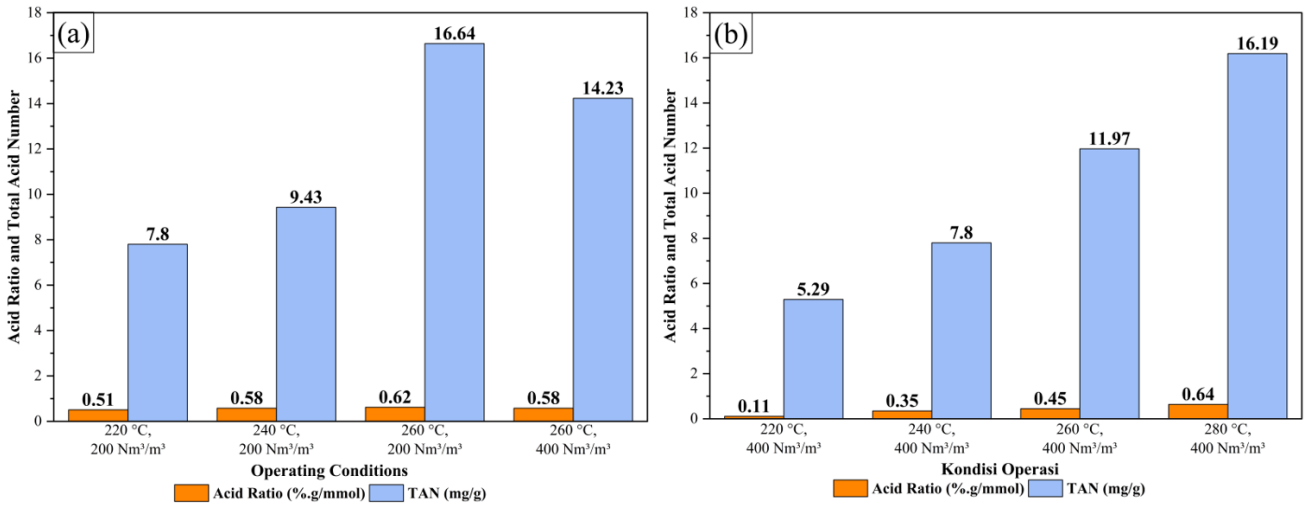


Figure 6. Acid ratio and total acid number: (a) Pt/γ-Al_2O_3-Cl (b) Pt/Sn(0.4)-γ-Al_2O_3-B.

Copyright © 2027, ISSN 1978-2993

The complexity of the FAME hydrogenation reaction network, along with its various competing pathways, is presented in Figure 8. The observed by-product distribution confirms that FAME hydrogenation did not proceed through a single pathway, but instead involved several competing routes: the main pathway of carbonyl hydrogenation toward aldehyde and fatty alcohol; subsequent pathways including dehydrogenation back to aldehyde, dehydration to alkene, esterification to wax ester, and intermolecular dehydration to ether; as well as side pathways from FAME, including hydrodeoxygenation or decarboxylation to alkane, hydrolysis to fatty acid, and double-bond isomerization to ester isomers [5,68]. This competition among pathways explains the broad product distribution and the still-limited fatty alcohol yield observed in both catalyst systems.

4. Conclusions

The incorporation of Sn and B into γ-Al_2O_3 resulted in changes in the physicochemical properties of the support. Compared with pure γ-Al_2O_3, the modified supports exhibited smaller crystallite sizes and lower crystallinity. However, the crystallite size showed a non-monotonic trend with increasing Sn loading, reaching its minimum at 0.4% Sn. The surface area increased

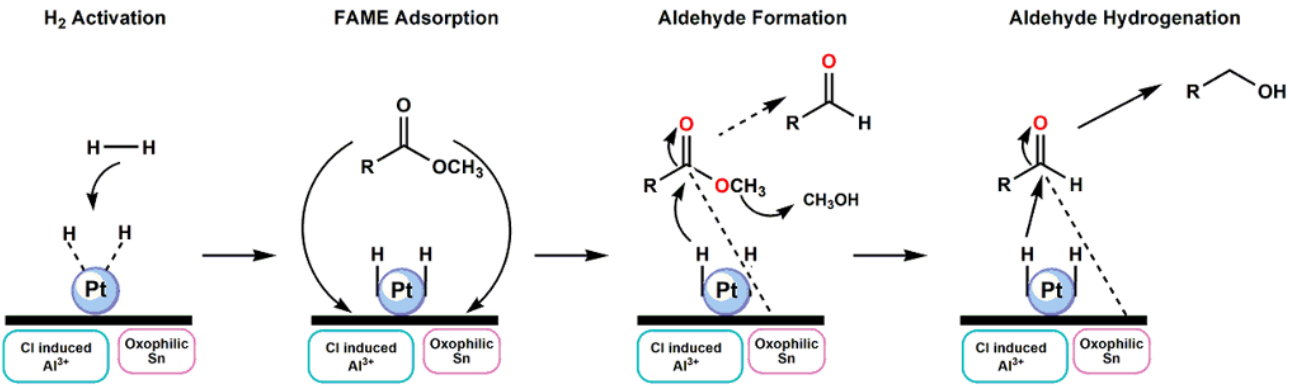


Figure 7. Mechanism of the FAME hydrogenation reaction over the catalyst [49,67].

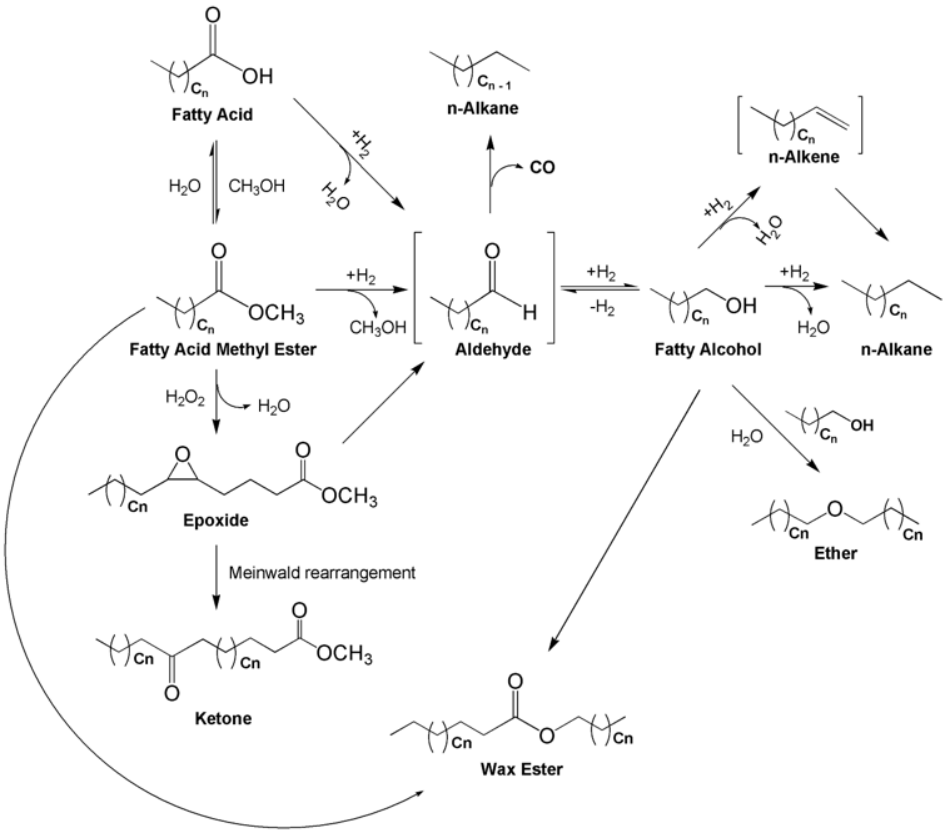


Figure 8. Reaction scheme of FAME hydrogenation reaction [5,68].

Copyright © 2027, ISSN 1978-2993

after Sn–B modification and remained relatively stable across the investigated Sn loadings, while the average pore diameter decreased consistently. The pore volume increased relative to the pure support but decreased slightly with increasing Sn concentration. Furthermore, the total acidity of the Pt/Sn-γ-Al_2O_3-B catalysts exhibited a non-monotonic variation, with the highest value observed at 0.4% Sn and a lower value at 0.6% Sn. The strong acid sites were predominant in the catalyst containing 0.6% Sn. Increasing Sn loading also influenced the catalyst reduction temperature.

CRediT Author Statement

Authors Contributions: A. F. Faqihah: Investigation, formal analysis, writing original draft. D. Sukandar: Conceptualization, methodology, supervision. W. Rustyawan: Supervision, resources. T. Rudiana: supervision A. Adawiah: Writing - review & editing. S. Suhendra: Project administration. All authors have read and agreed to the published version of the manuscript.

Conflict of (Competing) Interest Statement

The authors declare that they have no known competing financial interests or personal relationships that could have appeared to influence the work reported in this paper.

Acknowledgements

The authors would like to thank UIN Syarif Hidayatullah Jakarta for the financial support provided for this research under grant number B-41.a/LP2M.1/PT.01.03/06/2026, as well as PT Pertamina Research and Technology Innovation (RTI), Pulogadung, East Jakarta, for providing laboratory facilities and technical support during this research.

Declaration of Generative AI Use

During the preparation of this manuscript, the authors used DeepL to assist with translation, ChatGPT (OpenAI) to support the formulation and refinement of manuscript text and responses to reviewer comments, and Grammarly to check grammar, spelling, and language clarity. All AI-assisted outputs were reviewed, verified, and edited by the authors to ensure their accuracy and consistency with the experimental results. The authors take full responsibility for the content, interpretation of the data, and final version of this manuscript.

References

[1] GAPKI. (2025). GAPKI News Menggali Solusi Kompleksitas Industri Sawit. *GAPKI Pusat*.

[2] Joseph, G.H., Kindangen, J.G., Paat, P.C., Taulaby, D. (2022). Opportunities for the Development of The Oleochemical Industry of Coconut Products. *E3S Web of Conferences*, *361*, 02024. DOI: 10.1051/e3sconf/202236102024

[3] Yoyo, T., Hanitha, V., Hendra, H. (2023). Developing The Competitiveness Model of The Palm Oil-Based Fatty Acid and Fatty Alcohol Industry in Indonesia Using Porter's Diamond Cluster Competitiveness Model. *Primanomics : Jurnal Ekonomi & Bisnis*, *21*(1), 13–23. DOI: 10.31253/pe.v21i1.1537

[4] Salaheldeen, M., Mariod, A.A., Aroua, M.K., Rahman, S.M.A., Soudagar, M.E.M., Fattah, I.M.R. (2021). Current State and Perspectives on Transesterification of Triglycerides for Biodiesel Production. *Catalysts*, *11*(9), 1121. DOI: 10.3390/catal11091121

[5] Belousov, A.S., Esipovich, A.L., Kanakov, E.A., Otopkova, K.V. (2021). Recent advances in sustainable production and catalytic transformations of fatty acid methyl esters. *Sustainable Energy & Fuels*, *5*(18), 4512–4545. DOI: 10.1039/D1SE00830G

[6] Hammad, W.A., Hawash, S.A., Abdel-latif, M.S., Kuku, M., Amr, M.H.A. (2025). High efficiency adsorption of hexavalent chromium using bioderived activated carbon kinetics, isotherms, and thermodynamics. *Scientific Reports*, *15*(1), 25871. DOI: 10.1038/s41598-025-08472-7

[7] Shesterkina, A., Strekalova, A., Mashkin, M., Mishin, I., Vikanova, K., Tursunov, O., Dunaev, S., Kustov, A. (2025). Influence of the Support Nature of Copper Catalysts on Catalytic Properties in the Hydrogenation of Fatty Acid Esters. *International Journal of Molecular Sciences*, *26*(7), 3289. DOI: 10.3390/ijms26073289

[8] Zhang, K., Zhang, H., Ma, H., Ying, W., Fang, D. (2015). The effect of preparation method on the performance of PtSn/Al 2 O 3 catalysts for acetic acid hydrogenation. *Polish Journal of Chemical Technology*, *17*(1), 11–17. DOI: 10.1515/pjct-2015-0003

[9] Pritchard, J., Ciftci, A., Verhoeven, M.W.G.M. (Tiny), Hensen, E.J.M., Pidko, E.A. (2017). Supported Pt-Re catalysts for the selective hydrogenation of methyl and ethyl esters to alcohols. *Catalysis Today*, *279*, 10–18. DOI: 10.1016/j.cattod.2016.03.043

[10] Brijaldo, M.H., Rojas, H.A., Xing, Y., Passos, F.B., Martínez, J.J. (2024). Pt/Nb2O5-Al2O3 Catalysts for the Hydrogenation and Reductive Amination of Furfural. *Catalysts*, *14*(8), 493. DOI: 10.3390/catal14080493

Copyright © 2027, ISSN 1978-2993

[11] Wang, Y., Wang, Z., Xu, C., Zhou, S. (2023). Synthesis of Alumina Supported Pt-SnO2 Hybrid Nanostructures by In Situ Transformation of PtSn Alloy Nanoparticles and Their Application as Highly Efficient Catalysts for Selective Hydrogenation of Furfural. *The Journal of Physical Chemistry C*, *127*(8), 4033–4041. DOI: 10.1021/acs.jpcc.2c07661

[12] Sánchez, M.A., Vicerich, M.A., Fonseca Benítez, C., Nardi, F., Passamonti, F.J., Mazzieri, V.A. (2024). Selective hydrogenation of biomass-derived fatty acid methyl esters to fatty alcohols on RuSn–B/Al2O3 catalysts: analysis of the operating conditions and kinetics. *Reaction Kinetics, Mechanisms and Catalysis*, *137*(4), 2173–2195. DOI: 10.1007/s11144-024-02661-7

[13] Mazzieri, V.A., Sad, M.R., Vera, C.R., Pieck, C.L., Grau, R. (2010). Preparation and characterization oF Ru-Sn/Al2O3 catalysts for the hydrogenation of fatty acid methyl esters. *Química Nova*, *33*(2), 269–272. DOI: 10.1590/S0100-40422010000200007

[14] Jiao, J., Yang, Y., Yuan, M., Tang, X., Shi, M., He, K., Zhang, H., Bi, Y., Qin, Y., Song, L. (2025). Coke deposition mechanisms of propane dehydrogenation on different sites of Al_2O_3 supported PtSn catalysts. *Chemical Synthesis*, *5*(1). DOI: 10.20517/cs.2024.43

[15] Feng, R., Yan, X., Hu, X. (2018). Effects of boron and fluorine modified γ-Al2O3 with tailored surface acidity on catalytic ethanol dehydration to ethylene. *Journal of Porous Materials*, *25*(4), 1105–1114. DOI: 10.1007/s10934-017-0522-y

[16] Aly, M., Fornero, E.L., Leon-Garzon, A.R., Galvita, V.V., Saeys, M. (2020). Effect of Boron Promotion on Coke Formation during Propane Dehydrogenation over Pt/γ-Al_2O_3 Catalysts. *ACS Catalysis*, *10*(9), 5208–5216. DOI: 10.1021/acscatal.9b05548

[17] Taghizadeh Yusefabad, E., Tavasoli, A., Zamani, Y. (2021). Influence of the Borate on the Performance of ASA-Al2O3 supported Ni-Mo Hydrocracking Catalyst. *J. Chem. Chem. Eng. Research Article*, *40*(4). DOI: 10.30492/ijcce.2020.39173.

[18] Pertamina. (2015). *Katalis-Dasar Teori dan Metode Uji*. Pertamina.

[19] Shi, F., Liang, F., Wei, Y., Wu, J., Huang, S., Wang, H., Wang, Z., Shi, G. (2026). Experimental and DFT studies on the preparation of boron-doped Pd/Al2O3 foam ceramic-based catalysts for mirabelon intermediates. *Applied Catalysis A: General*, *710*, 120704. DOI: 10.1016/j.apcata.2025.120704

[20] Zhang, Z., Zhu, Y., Asakura, H., Zhang, B., Zhang, J., Zhou, M., Han, Y., Tanaka, T., Wang, A., Zhang, T., Yan, N. (2017). Thermally stable single atom Pt/m-Al2O3 for selective hydrogenation and CO oxidation. *Nature Communications*, *8*(1), 16100. DOI: 10.1038/ncomms16100

[21] Fu, R. (2021). The Preparation of Boron-doped Activated Alumina by impregnating boron in the period of boehmite. *MATEC Web of Conferences*, *353*, 01026. DOI: 10.1051/matecconf/202135301026

[22] Pham, H.N., Sattler, J.J.H.B., Weckhuysen, B.M., Datye, A.K. (2016). Role of Sn in the Regeneration of Pt/γ-Al2O3 Light Alkane Dehydrogenation Catalysts. *ACS Catalysis*, *6*(4), 2257–2264. DOI: 10.1021/acscatal.5b02917

[23] Wang, X., Cui, J., Zhang, N., Song, J., Fan, X., Zhao, Z., Kong, L., Xiao, X., Xie, Z. (2022). Propane Dehydrogenation over PtSn/Al2O3 Catalysts: Influence of Urea to Al(NO3)3·9H2O Ratio. *Catalysts*, *12*(2), 157. DOI: 10.3390/catal12020157

[24] Slavinskaya, E.M., Kibis, L.S., Stonkus, O.A., Svintsitskiy, D.A., Stadnichenko, A.I., Fedorova, E.A., Romanenko, A.V., Marchuk, V., Doronkin, D.E., Boronin, A.I. (2021). The Effects of Platinum Dispersion and Pt State on Catalytic Properties of Pt/Al_2O_3 in NH_3 Oxidation. *ChemCatChem*, *13*(1), 313–327. DOI: 10.1002/cctc.202001320

[25] Jafar Tafreshi, M., Masoomi Khanghah, Z. (2015). Infrared Spectroscopy Studies on sol-gel prepared alumina Powders. *Materials Science*, *21*(1). DOI: 10.5755/j01.ms.21.1.4872

[26] Schöneborn, M., Werner, J., Harmening, T., Weirich, T.E. (2022). Advances in the understanding of mesoporous transition aluminas: Unveiling the correlation between morphology and thermostability. *Journal of Solid State Chemistry*, *308*, 122906. DOI: 10.1016/j.jssc.2022.122906

[27] Delmastro, A., Gozzelino, G., Mazza, D., Vallino, M., Busca, G., Lorenzelli, V. (1992). Characterization of microporous amorphous alumina–boria. *J. Chem. Soc., Faraday Trans.*, *88*(14), 2065–2070. DOI: 10.1039/FT9928802065

[28] Mardkhe, M.K., Huang, B., Bartholomew, C.H., Alam, T.M., Woodfield, B.F. (2016). Synthesis and characterization of silica doped alumina catalyst support with superior thermal stability and unique pore properties. *Journal of Porous Materials*, *23*(2), 475–487. DOI: 10.1007/s10934-015-0101-z

[29] Abi Aad, J., Courty, P., Decottignies, D., Michau, M., Diehl, F., Carrier, X., Marceau, E. (2017). Inhibition by Inorganic Dopants of γ-Alumina Chemical Weathering under Hydrothermal Conditions: Identification of Reactive Sites and their Influence in Fischer–Tropsch Synthesis. *ChemCatChem*, *9*(12), 2106–2117. DOI: 10.1002/cctc.201700140

[30] Jang, M.G., Yoon, S., Shin, D., Kim, H.J., Huang, R., Yang, E., Kim, J., Lee, K.-S., An, K., Han, J.W. (2022). Boosting Support Reducibility and Metal Dispersion by Exposed Surface Atom Control for Highly Active Supported Metal Catalysts. *ACS Catalysis*, *12*(8), 4402–4414. DOI: 10.1021/acscatal.2c00476

Copyright © 2027, ISSN 1978-2993

[31] Rusdan, N.A., Timmiati, S.N., Isahak, W.N.R. W., Yaakob, Z., Lim, K.L., Khaidar, D. (2022). Recent Application of Core-Shell Nanostructured Catalysts for CO2 Thermocatalytic Conversion Processes. *Nanomaterials*, *12*(21), 3877. DOI: 10.3390/nano12213877

[32] Zhang, C., Gao, Y., Zhang, J., Chen, Y., Zhu, Q., Jiao, Y., Wang, J., Chen, Y., Li, X. (2023). Optimizing Ni dispersion and stability over SiO2 supported Ni–La2O3 catalysts by preparation method for enhancing H2 selectivity and durability on steam reforming of methylcyclohexane. *Journal of Power Sources*, *555*, 232340. DOI: 10.1016/j.jpowsour.2022.232340

[33] Singh, J., Kaur, N., Kaur, P., Kaur, S., Kaur, J., Kukkar, P., Kumar, V., Kukkar, D., Rawat, M. (2018). Piper betle leaves mediated synthesis of biogenic SnO2 nanoparticles for photocatalytic degradation of reactive yellow 186 dye under direct sunlight. *Environmental Nanotechnology, Monitoring & Management*, *10*, 331–338. DOI: 10.1016/j.enmm.2018.07.001

[34] Lampman, S. (2019). X-Ray Spectroscopy[1]. In *Materials Characterization* (pp. 337–361). ASM International. DOI: 10.31399/asm.hb.v10.a0006645

[35] Robbika, O.I., Rohyami, Y., Hadriansyah, H. (2022). Critical Quality Control on Determination of Boron Using ICP-OES with Gravimetric Method. *IJCA (Indonesian Journal of Chemical Analysis)*, *5*(2), 103–110. DOI: 10.20885/ijca.vol5.iss2.art5

[36] Williams, J.H., Zheng, Q., Mantle, M.D., Sederman, A.J., Gladden, L.F. (2023). Probing the Diffusion Mechanism of *n* -Alkanes in Mesoporous Confinement Using Pulsed Field Gradient NMR. *The Journal of Physical Chemistry C*, *127*(31), 15326–15335. DOI: 10.1021/acs.jpcc.3c02793

[37] Zheng, W., Yamada, S.A., Hung, S.T., Sun, W., Zhao, L., Fayer, M.D. (2020). Enhanced Menshutkin S_N2 Reactivity in Mesoporous Silica: The Influence of Surface Catalysis and Confinement. *Journal of the American Chemical Society*, *142*(12), 5636–5648. DOI: 10.1021/jacs.9b12666

[38] Shen, H., Li, H., Yang, Z., Li, C. (2022). Magic of hydrogen spillover: Understanding and application. *Green Energy & Environment*, *7*(6), 1161–1198. DOI: 10.1016/j.gee.2022.01.013

[39] Shi, W., Oda, A., Yamamoto, Y., Harada, S., Ohtsu, T., Sawabe, K., Satsuma, A. (2025). Encapsulated Platinum–Tin Nanoparticles in Silicalite-1 Zeolite for Methylcyclohexane Dehydrogenation. *ACS Sustainable Chemistry & Engineering*, *13*(9), 3608–3621. DOI: 10.1021/acssuschemeng.4c09762

[40] Arena, F., Dario, R., Parmaliana, A. (1998). A characterization study of the surface acidity of solid catalysts by temperature programmed methods. *Applied Catalysis A: General*, *170*(1), 127–137. DOI: 10.1016/S0926-860X(98)00041-6

[41] Li, X., Li, J., Yuan, M., Li, N., Xu, J., Wang, G., Li, C. (2023). Effect of chlorine on the performance of Cr-K/γ-Al2O3 catalyst for n-hexane dehydrogenation. *Applied Catalysis A: General*, *664*, 119322. DOI: 10.1016/j.apcata.2023.119322

[42] Yang, E., Jang, E.J., Lee, J.G., Yoon, S., Lee, J., Musselwhite, N., Somorjai, G.A., Kwak, J.H., An, K. (2018). Acidic effect of porous alumina as supports for Pt nanoparticle catalysts in *n* -hexane reforming. *Catalysis Science & Technology*, *8*(13), 3295–3303. DOI: 10.1039/C8CY00776D

[43] Mazzieri, V.A., Grau, J.M., Vera, C.R., Yori, J.C., Parera, J.M., Pieck, C.L. (2005). Role of Sn in Pt–Re–Sn/Al2O3–Cl catalysts for naphtha reforming. *Catalysis Today*, *107–108*, 643–650. DOI: 10.1016/j.cattod.2005.07.042

[44] Yang, H., Wang, X., Wang, H., Xie, Y., Lu, A. (2025). Coprecipitation of Sn and Al Precursors to Create Additional Acid Sites of Pt/Sn-Al_2O_3 Catalysts for Propane Dehydrogenation. *ChemCatChem*, *17*(3). DOI: 10.1002/cctc.202401603

[45] Ali, A.M., Zahrani, A.A., Daous, M.A., Podila, S., Alshehri, M.K., Rather, S., Saeed, U. (2022). Sequential and/or Simultaneous Wet-Impregnation Impact on the Mesoporous Pt/Sn/Zn/γ-Al_2O_3 Catalysts for the Direct Ethane Dehydrogenation. *Journal of Nanomaterials*, *2022*(1). DOI: 10.1155/2022/8739993

[46] Keivanimehr, F., Kabiri, R., Habibzadeh, S., Mokhtarian, M. (2025). Dual rare earth-doped Pt–Sn/Al2O3 catalysts with synergistic Ce and Sm effects on high-efficiency aromatization and coke suppression in naphtha reforming. *Scientific Reports*, *15*(1), 19910. DOI: 10.1038/s41598-025-04371-z

[47] Cordero-Lanzac, T., Palos, R., Hita, I., Arandes, J.M., Rodríguez-Mirasol, J., Cordero, T., Bilbao, J., Castaño, P. (2018). Revealing the pathways of catalyst deactivation by coke during the hydrodeoxygenation of raw bio-oil. *Applied Catalysis B: Environmental*, *239*, 513–524. DOI: 10.1016/j.apcatb.2018.07.073

[48] Jiao, J., Yang, Y., Yuan, M., Tang, X., Shi, M., He, K., Zhang, H., Bi, Y., Qin, Y., Song, L. (2025). Coke deposition mechanisms of propane dehydrogenation on different sites of Al_2O_3 supported PtSn catalysts. *Chemical Synthesis*, *5*(1). DOI: 10.20517/cs.2024.43

[49] Sánchez, M.A., Mazzieri, V.A., Vicerich, M.A., Vera, C.R., Pieck, C.L. (2015). Ru-Sn-B/Al_2O_3 Catalysts for Selective Hydrogenation of Methyl Oleate: Influence of the Ru/Sn Ratio. *Journal of Chemistry*, *2015*(1). DOI: 10.1155/2015/561350

[50] Oenema, J., van Alst, R.A., Meijerink, M.J., Zečević, J., de Jong, K.P. (2020). The Influence of Residual Chlorine on Pt/Zeolite Y/γ-Al2O3 Composite Catalysts: Acidity and Performance. *Applied Catalysis A: General*, *605*, 117815. DOI: 10.1016/j.apcata.2020.117815

Copyright © 2027, ISSN 1978-2993

[51] Lee, C.-J., Shee, N.K., Kim, H.-J. (2023). Fabrication and properties of Sn(iv) porphyrin-linked porous organic polymer for environmental applications. *RSC Advances*, *13*(34), 24077–24085. DOI: 10.1039/D3RA04117D

[52] Fonseca Benítez, C.A., Mazzieri, V.A., Sánchez, M.A., Benitez, V.M., Pieck, C.L. (2019). Selective hydrogenation of oleic acid to fatty alcohols on Rh-Sn-B/Al2O3 catalysts. Influence of Sn content. *Applied Catalysis A: General*, *584*, 117149. DOI: 10.1016/J.APCATA.2019.117149

[53] Ábrahám, E., Varga, K., Almási, B., Turczel, G., Erdélyi, Á., Farkas, V., Osterthun, O., Nagy, T., Klankermayer, J., Bényei, A., Nagyházi, M., Tuba, R. (2025). Synthesis of 16-Electron $RuHCl(CO)(PPh_3)_2$ Catalyst Rendering Superior C═C Double Bond Isomerization Activity. *ChemCatChem*, *17*(11). DOI: 10.1002/cctc.202500100

[54] Kepp, K.P. (2016). A Quantitative Scale of Oxophilicity and Thiophilicity. *Inorganic Chemistry*, *55*(18), 9461–9470. DOI: 10.1021/acs.inorgchem.6b01702

[55] Muchave, G.J., Almeida, J.M.A.R., Aranda, D.A.G. (2022). Hydrogenation of Palm Esters to Fatty Alcohols using Re/Nb/Al2O3 Catalysts. *International Journal of Science and Research (IJSR)*, *11*(6), 516–531. DOI: 10.21275/SR22530015241

[56] Trinh, T.-K.-H., de Hemptinne, J.-C., Lugo, R., Ferrando, N., Passarello, J.-P. (2016). Hydrogen Solubility in Hydrocarbon and Oxygenated Organic Compounds. *Journal of Chemical & Engineering Data*, *61*(1), 19–34. DOI: 10.1021/acs.jced.5b00119

[57] Ivaniš, G., Fele Žilnik, L., Pomeroy, B., Likozar, B., Grilc, M. (2022). Solubility of hydrogen or oxygen in biomass-derived lipid, carbohydrate and lignin chemicals: From experiments to thermodynamic equilibria modelling. *Fluid Phase Equilibria*, *559*, 113494. DOI: 10.1016/j.fluid.2022.113494

[58] Qureshi, M.S., Touronen, J., Uusi-Kyyny, P., Richon, D., Alopaeus, V. (2016). Solubility of hydrogen in bio-oil compounds. *The Journal of Chemical Thermodynamics*, *102*, 406–412. DOI: 10.1016/j.jct.2016.07.010

[59] Aslam, R., Müller, K., Müller, M., Koch, M., Wasserscheid, P., Arlt, W. (2016). Measurement of Hydrogen Solubility in Potential Liquid Organic Hydrogen Carriers. *Journal of Chemical & Engineering Data*, *61*(1), 643–649. DOI: 10.1021/acs.jced.5b00789

[60] Anoop, A.A., Ramees, P.M., Ragavan, K.V. (2025). Coconut oleosomes as a sustainable ingredient for food emulsion systems. *Sustainable Food Technology*, *3*(4), 1164–1174. DOI: 10.1039/D5FB00112A

[61] Sagar, K.M.A., Venudharan, V. (2026). Development of FTIR-based quantitative framework for rejuvenator selection in recycled asphalt applications. *Construction and Building Materials in Transportation*, *1–2*, 100012. DOI: 10.1016/J.JCBMTR.2026.100012

[62] Smith, B.C. (2022). The Infrared Spectra of Polymers, VI: Polymers With C-O Bonds. *Spectroscopy*, 15-19,27. DOI: 10.56530/spectroscopy.ly3071f5

[63] Yang, Z.-C., Zhang, P., Guo, Z.-X. (2026). Synthesis of Unsymmetrical Dialkyl Ethers via Direct Etherification Cocatalyzed Using $FeCl_3.6H_2O$ and 1,1,1,3,3,3-Hexafluoroisopropanol. *ACS Omega*, *11*(1), 1927–1934. DOI: 10.1021/acsomega.5c10269

[64] Peters, M.A., Alves, C.T., Wang, J., Onwudili, J. A. (2022). Subcritical Water Hydrolysis of Fresh and Waste Cooking Oils to Fatty Acids Followed by Esterification to Fatty Acid Methyl Esters: Detailed Characterization of Feedstocks and Products. *ACS Omega*, *7*(50), 46870–46883. DOI: 10.1021/acsomega.2c05972

[65] Hoffmann, M.M., Gonzalez, A.A., Huynh, M.T., Miller, K.K., Gutmann, T., Buntkowsky, G. (2024). Densities, Viscosities, and Self-Diffusion Coefficients of Octan-1-ol and Related Ether-Alcohols. *Journal of Chemical & Engineering Data*, *69*(8), 2688–2699. DOI: 10.1021/acs.jced.4c00195

[66] Feng, G., Gao, M., Wang, L., Chen, J., Hou, M., Wan, Q., Lin, Y., Xu, G., Qi, X., Chen, S. (2022). Dual-resolving of positional and geometric isomers of C=C bonds via bifunctional photocycloaddition-photoisomerization reaction system. *Nature Communications*, *13*(1), 2652. DOI: 10.1038/s41467-022-30249-z

[67] Li, P., Zhang, M., Wang, S., Yu, H., Wu, J., Yang, L., Xu, G. (2023). Pd–Ni–Fe Nanoparticles Supported on UiO-66 for Selective Hydrogenation of Fatty Acid Methyl Esters to Alcohols. *ACS Applied Nano Materials*, *6*(20), 18892–18904. DOI: 10.1021/acsanm.3c03297

[68] Quintero-Ramos, D., Checa, M., Jordá, J.L., Sabater, M.J. (2023). Study on the Hydrogenation of Ethyl Stearate to the Fatty Alcohol 1-Octadecanol over Ru on Tungstated Zirconia. *Catalysts*, *13*(10), 1362. DOI: 10.3390/catal13101362

Copyright © 2027, ISSN 1978-2993